Final Report

Processing and microstructural characterization of cold sintered ceramics

Abdullah Jabr

Supervisor MUL: Raul Bermejo

Supervisor PSU: Clive Randall

Table of Contents

Project Description

Ceramics are recognized as strong candidate materials for modern advanced applications, owing to their outstanding mechanical, chemical and high-temperature resistance. However, such high stability poses difficulties in their fabrication process, limiting it to powder-based routes where high temperatures, typically higher than 1000°C, are applied. Therefore, ceramic fabrication results in high energy consumption, carbon footprint and costs. Recently, an ultralow-temperature densification process, which allows densifying ceramics at temperatures not exceeding 300°C down to room temperature, was introduced by Professor Clive Randall and his research group at the Pennsylvania State University (PSU). This process has been termed "Cold Sintering Process" and has the potential to transform ceramic industry into a green and sustainable industry. The research done in this project was carried out in collaboration with Professor Randall's research group at the Materials Research Institute at the Pennsylvania state university within a period of 4 months. The work was focussed on the fabrication and characterization of ZnO ceramic systems processed at low temperatures using the cold sintering process (CSP). The characterization included chemical, microstructural as well as mechanical analysis. The aim of this research was to explore the effect of the processing parameters, such as liquid phase chemistry and temperature, on the microstructure and mechanical properties of cold sintered ZnO.

Abstract

Cold sintering is a chemomechanical assisted densification process which allows densifying ceramics at low temperatures not exceeding 300 °C. This substantial reduction in the sintering temperature is accomplished by the aid of an externally applied pressure and a compatible transient liquid phase. In this paper, ZnO was cold sintered using deionized water and different organic acids, having an increasing solubility for ZnO in the following order: acetic, formic, and citric acid. The effect of these different transient phases on densification, transient chemical changes, microstructural evolution and mechanical response of the cold sintered samples was all investigated. To explain the chemical effects, Fourier transform infrared spectroscopy (FTIR), thermogravimetric analyses (TGA) and transmission electron microscopy (TEM) were conducted. The results show that high relative densities (~ 96%) are

achieved by formic and acetic acid, while poor densification is observed for citric acid (< 80%), despite the much higher solubility of the later. This is explained in terms of the stability of the carboxylates formed by the respective liquid phases, which highlights the importance of the precipitation step during the cold sintering process. The biaxial characteristic strength of samples cold sintered using formic and acetic acid was 88 MPa and 36 MPa, respectively. The relatively higher strength achieved by formic acid is 40% higher than the previously reported value in the literature.

1 Introduction

Conventionally, ceramics are manufactured by thermal treatment of a shaped powder compact at temperatures in the range of 50% to 80% of the melting point of the material. Since ceramics are characterized by a high melting point, these temperatures are usually higher than 1000°C [1]. The use of such high temperatures results in deleterious effects such as thermal stresses, loss of volatile elements, reaction/diffusion between different phases, among other economical and ecological concerns related to energy consumption and carbon emissions. Thus, co-integration of metals, polymers, and ceramics, which is aspired in multifunctional components is not accessible by conventional sintering methods. Therefore, lowering the sintering temperature of ceramics has been the incentive for developing new sintering techniques. While reducing surface energy is the driving force in conventional sintering, modern techniques, such as hot pressing, Field-Assisted Sintering (FAST) and liquid phase sintering, seek to activate densification at lower temperatures through application of external pressure [2], electric field [3] or addition of a liquid phase [4]. Although much progress has been achieved in reducing the sintering temperature, most of these techniques still operate at temperatures higher than those required for co-sintering of complex composite materials.

In 2016, the cold sintering process (CSP) was introduced, which allows densification of ceramics at unprecedented low temperatures below 300°C [5]. This substantial reduction of the sintering temperature is enabled by an external pressure and a transient liquid phase that provides a faster diffusion path for ionic species and drives mechanisms such as particle rearrangement, dissolution and precipitation, and in some cases grain growth and recrystallization [6–8]. The chemomechanical process that can drive these densification and precipitation processes is known as pressure solution creep [9]. CSP unlocked new design strategies and materials combinations which were unfeasible previously, such as co-integration of ceramics with polymers, nanomaterials and also metals [10–12].

The mechanisms operating during cold sintering have been extensively studied on ZnO, which is commonly used as a model system in sintering studies. Funahashi et al. [8] densified ZnO to relative densities higher than 90% using aqueous solution of acetic acid at temperatures well below 300°C. However, no densification was achieved when pure water was used (only 65% relative density), as ZnO is regarded as insoluble in water. These results indicated the

importance of the solubility of the solid phase into the transient liquid phase which provides Zn^{2+} cations that diffuse from highly stressed contact areas between the particles (high chemical potential) to pore surfaces (low chemical potential) in the dissolution-precipitation step, driving the elimination of pores and densification. Experiments by Kang et al. [13] showed that dissolution of ZnO into the liquid phase is not a prerequisite for cold sintering and that high densities (>98%) can still be achieved if the liquid phase is presaturated with Zn^{2+} cations as in zinc acetate solution, albeit the pH value of 7, where ZnO is regarded as insoluble. Previous studies have reported an adverse effect of high acetic acid concentration in the liquid phase on densification in CSP of ZnO. Despite the higher dissolution capability, the reported densities were 88% for 9 M [14] and 70% for 17.5 M acetic acid [8], indicating the importance of the role of water in CSP. Sengul et al. [14] proposed a theoretical explanation of the role of water using Reactive force field modelling (ReaxFF). The model showed that water hydroxylates the surface of ZnO, forming bridging hydroxyl groups which facilitate adsorption, diffusion, and hence, recrystallization of Zn^{2+} cations on the surface of ZnO. An excess of acetic acid would act as a diffusion barrier and occupy surface sites, which otherwise would have been available as recrystallization sites. Floyd et al. [15] investigated the effect of humidity on the CSP of ZnO using a solid transport phase of zinc acetate dihydrate containing only structural water. In their experiments, almost full densification was only achieved under processing conditions with more than 50% relative humidity, demonstrating the role of small amounts of adsorbed water to drive mass transport through water-enhanced diffusion. Another important aspect is the interface reaction between the solid and liquid phase, as investigated in the experiments by Ndayishimiye et al. [16], where an aqueous solution of metal–organic chelate (zinc acetylacetonate hydrate) was used as a transient liquid phase. The result was dense ZnO with relative densities higher than 90%. The proposed mechanism involved the hydrolysis of the chelate in water and its dynamic interaction with ZnO surfaces, leading to its precipitation onto ZnO. Nevertheless, this approach works for metal–organic chelates that have high propensity to transform into ZnO and exhibit fast hydrolysis.

Based on these investigations, several important factors associated with the role of the liquid phase for cold sintering ZnO can be deduced: a) the presence of water, b) the solubility of ZnO in the liquid phase to generate Zn^{2+} cations that can participate in the dissolution–precipitation step, or alternatively preloading the liquid phase with the cations, and c) the

good chelating ability while maintaining low stability to promote back transformation to ZnO. In this work, we propose an aqueous solution of formic acid as transient liquid phase for CSP, which meets all the mentioned requirements with the advantage of being the simplest organic acid with lowest carbon content. The aim of this study is to investigate the effect of liquid phase selection on both densification, microstructure and mechanical response of cold sintered samples. In order to explain different chemical mechanisms, the results obtained with formic acid are compared to samples cold sintered with acetic acid, which is commonly used for cold sintering ZnO. In addition, the results are also compared to samples sintered with water which has negligible solubility for ZnO and citric acid, in which ZnO is highly soluble.

Most studies on cold sintering have focused on evaluating the sinterability by measuring the density, or electrical performance in functional systems. However, studies on the mechanical performance of cold sintered materials are rather scarce. Lowum et al. [17] have investigated the biaxial strength of ZnO cold sintered with aqueous solution of zinc acetate using the-ball-on-three-balls test. They reported a characteristic strength of 65 MPa and a Weibull modulus of 8. The reported values were regarded to be low compared to values reported in the literature (strength between 80-120 MPa) for conventionally sintered ZnO. However, a direct comparison is not possible, since the strength values of conventionally sintered samples in the literature are measured under different testing configuration, using either three-point or four-point bending tests. A fractographic analysis that may explain the fracture behaviour of cold sintered samples is not found in the literature. Nur et al. [18] have investigated the mechanical properties of cold sintered ZnO on the micro-scale using nanoindentation and micropillar testing. The measured hardness and compressive strength were superior to those of conventionally sintered samples and comparable to single crystals. They found that the mechanical response of cold sintered ZnO to be influenced by preexisting stacking faults which annihilate in highly stressed regions at grain boundaries or amorphous regions. It has also been proposed that the use of water as a transient liquid phase is beneficial to avoid grain boundary etching and defect formation, which might occur when using acidic transient liquid phases. Nevertheless, this study is limited to the microscale which may not explain macroscopic mechanical response which is controlled by macroscopic defects and size effects.

The aim of this study is to investigate the effect of liquid phase selection on not only densification, as commonly reported, but on microstructure evolution and biaxial strength of cold sintered samples.

2 Experimental work

2.1 Starting materials

All cold sintering experiments were performed on a commercial ZnO powder provided by Alfa Aesar (NanoArc^{TM} ZN-0605) with a particle size between 40 and 100 nm. The transient liquid phases were prepared by diluting the pure acids to a concentration of 2 mol/l. In this study, the following pure acids were used: formic acid (reagent grade ≥95%, Sigma-Aldrich®), acetic acid (glacial ≥ 99.7%, VWR®) and citric acid (ACS reagent ≥ 99.0%, Sigma-Aldrich®).

2.2 Cold sintering process

First, 1 g of ZnO powder was mixed with 13 wt.% of the respective liquid phase in an agate mortar and pestle. The mixed powder was then filled into a stainless-steel die with a diameter of 13 mm. Uniaxial pressure was applied using a semiautomated press (Enerpac®) equipped with an extensometer (Keyence GT2-H32), which is capable of monitoring vertical displacements with a 0.5 μm resolution. More details on the setup of the press can be found in [19]. Heat was applied using a mica band heater with a power of 300 W (Tempco®) wrapped around the die. The temperature was controlled by a PID controller connected to the band heater and a J-type thermocouple placed in the centre of a custom designed bottom base plate (see Ref. [20] for more details) of the die which measures the process temperature and provides feedback for the PID controller, see Fig. 1a . CSP started by applying 335 MPa uniaxial pressure at room temperature for 5 minutes, then heating to the target temperature with a heating rate of 5°C/min. The dwell time for all experiments was 1 hour and it only accounts for the isothermal stage, i.e., after reaching the target temperature. All process parameters are summarised in Fig. 1b.
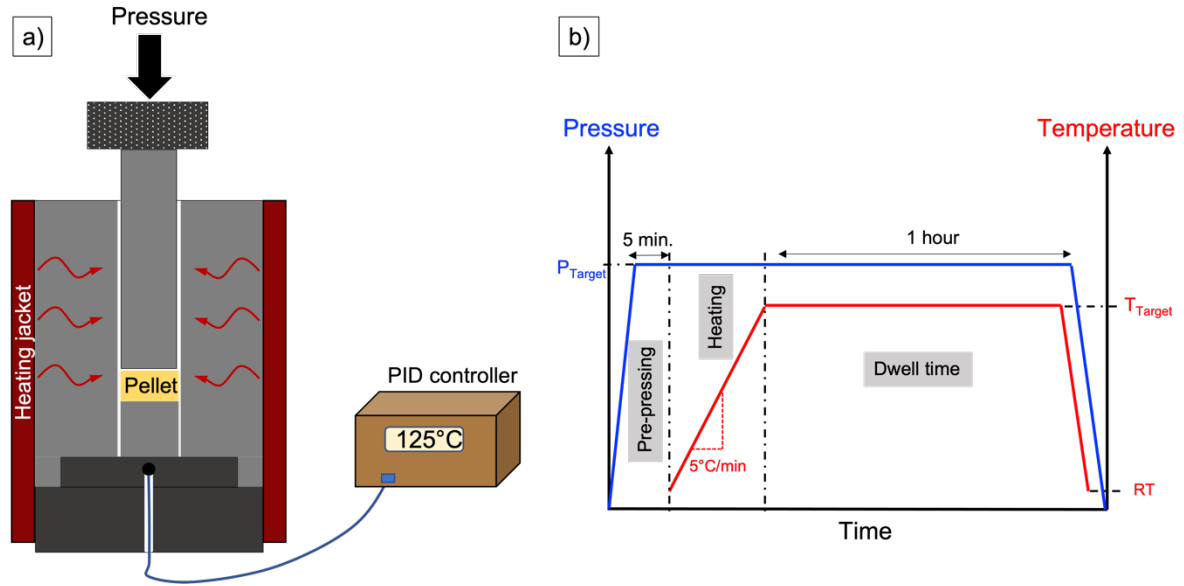
Figure 1: Experimental setup of the cold sintering process: (a) sintering die wrapped with a heating jacket and connected to a temperature controller through a thermocouple inserted in the bottom base plate, (b) temperature and pressure profile over time during CSP.

2.3 Characterization methods

The density was measured geometrically and using Archimedes principle according to EN 1389:2003 [21]. The geometrical density was calculated by dividing the sample mass, measured with 0.1 mg accuracy, by the volume as follows: $\rho_{geom} = \frac{m}{\pi \cdot r^2 \cdot h}$, where m is the sample mass, r is the radius and h is the thickness of the pellet. Geometrical density was evaluated for samples with open porosity, while Archimedes method was used for dense samples with no open porosity, using ethanol as immersion liquid. Relative densities are calculated as follows: $\rho_{rel} = \frac{\rho_{measured}}{\rho_{theoretical}}$, where $\rho_{theoretical}$ is the theoretical density of ZnO which was taken as 5.61 g/cm^3 [22]. Microstructural characterization was conducted using a field emission scanning electron microscope (Thermo Scientific™ Apreo 2 SEM) on fracture surfaces coated with 5 nm of iridium using a sputter coater (Leica EM ACE600 sputter coater). Average grain size was evaluated after measuring at least 700 grains.

Fourier transform infrared spectroscopy (FTIR) was conducted on the surface of cold sintered samples to identify any functional groups formed by the interaction between the transient liquid phase and ZnO. The measurements were carried out through attenuated total reflection (ATR) sampling geometry. The spectra were collected using a FT-IR spectrometer (Bruker Vertex 70) in the mid-IR spectral range (4000–500 cm^{-1}) with a resolution of 5 cm^{-1}.

The amount of residual organic content in the samples after CSP was determined by thermogravimetric analysis (TGA) using a thermal analyser (Netzsch STA 449 F3 Jupiter®). The measurements were performed between 20 and 600°C with a heating rate of 5°C/min.

2.4 Mechanical testing and fractography

The strength of cold sintered samples was measured under biaxial loading using the-ball-on-three-balls (B3B) test. In the B3B test setup, the sample is supported in the fixture by three balls on one side and the other side is centrally loaded by a fourth ball. All balls had a diameter of 9 mm, giving a support radius of 5.2 mm. The tests were conducted in universal testing machine (Model C43, MTS® criterion electromechanical test systems) equipped with a 1 kN load cell. Samples were tested in air at ambient conditions (~22°C and ~20% relative humidity). The test starts by applying a preload of 5 N ensure contact between the balls and the samples. Then, the load is increased with a displacement rate of 0.5 mm/min until fracture of the specimen. The force at which fracture occurs is registered and used for stress calculation. The strength was evaluated by calculating the maximum stress endured by the sample, which occurs in the center of the tensile loaded side, using the following formula [23]:

$$\sigma_{max} = f(\frac{R_a}{R}, \frac{t}{R}, v) \cdot \frac{F}{t^2} \tag{1}$$

where F is the maximum load at fracture, t is the thickness of the pellet and f is a dimensionless factor that depends on the loading and specimen geometry and Poisson's ratio (v) of the material. R_a is the support radius, R is the specimen radius. For a specimen thickness of 1.4 mm and a Poisson's ratio of 0.34 for ZnO [24], the factor f is approximately 1.98. The characteristic strength (σ_0) was evaluated by fitting the data according to the two-parameter Weibull statistics using the Maximum-Likelihood-method [25,26].

Fractographic analyses were conducted on selected samples fractured in the B3B-tests to identify fracture origins and their location. Assessing fracture origins is important for revealing the underlying reason for the different fracture behaviour of the different set of samples. The fracture surfaces were gold coated using an Agrar sputter coater and observed under a SEM (JEOL JCM- 6000Plus, NeoscopeTM, JEOL Ltd., Tokyo, Japan). The size and location of critical defects were measured on SEM images using an image analysis software (Olympus stream motion).

3   Results and discussion

3.1   Density evolution

Zinc oxide pellets were cold sintered over a temperature range between room temperature and 250°C using four different aqueous solution of: formic, acetic, citric acid and deionized water. Density trends over cold sintering temperature for all liquid phases are shown in Fig. 2. At room temperature, the relative density of all samples is below 75%. This indicates that the temperature is too low for driving densification mechanisms and the density is only given by powder compaction and particle rearrangement which is aided by the liquid phase. In the case of pellets sintered with acetic acid solution, the density increases significantly with small temperature increase, reaching a plateau of ~ 95% at 70°C. This trend is in fair agreement with previous studies on ZnO cold sintered with acetic acid [13,20] with a slight difference in the temperatures that can be explained by the different heating rates, molarity of the used solution and/or location of the thermocouple in the CSP setup. A Similar trend is observed for samples sintered using formic acid, but at relatively higher temperatures, such that a relative density > 95% is obtained above 90°C. Citric acid shows the poorest densification behaviour among all liquid phases. It shows the lowest density at room temperature, which indicates poor lubrication and rearrangement process. The highest density achieved is 79% at 250°C. For samples sintered using deionized water, the density increases with temperature; however, no full densification could be achieved, and the density remains below 86% even at the highest sintering temperature of 250°C. This result is in agreement with previous studies where water has been used as a transient liquid phase in CSP [8,16]. However, it contradicts other studies which achieved densities higher than 95% for ZnO cold sintered with water using a spark plasma sintering (SPS) apparatus [27,28]. This discrepancy could be attributed to the effect of electric field in cold sintering experiments conducted in SPS machines. Liang et al. [29] demonstrated the effect of electric field on the densification of ZnO using acetic acid in a hybrid cold sintering/SPS approach. They showed that the application of an electrical current during cold sintering enhances mass transport of the liquid phase, resulting in relative densities > 98% at much reduced pressure and dwell time of 3.8 MPa and 5 min, respectively.
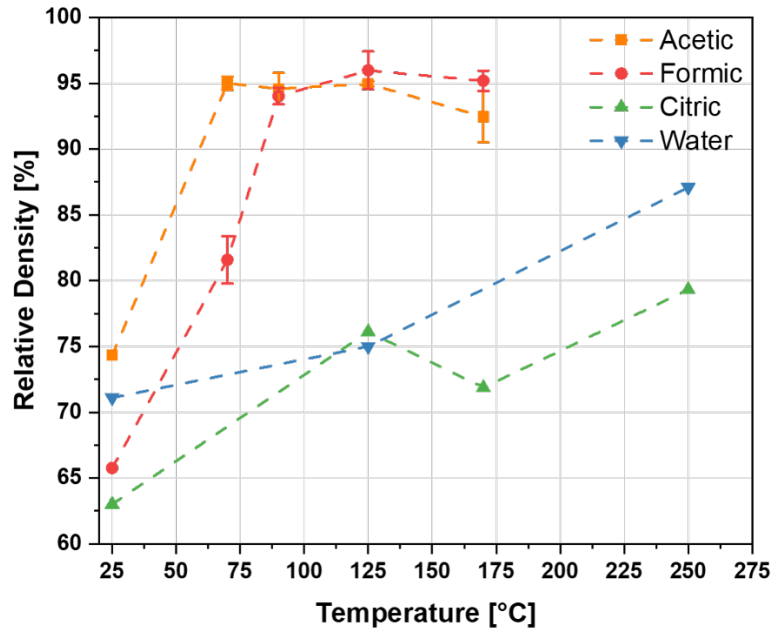
Figure 2: Relative density as a function of cold sintering temperature for pellets densified using aqueous solutions of acetic, formic, citric acid, and pure water.

3.2 Microstructure evolution

Further understanding of the densification behaviour can be made by characterizing microstructural changes during cold sintering at different temperatures. The selection of the temperature of interest was based upon in-situ measurement of the shrinkage during anisothermal heating to 250°C using the extensometer attached to the semiautomated press as described in the experimental section. Fig. 3a shows the linear shrinkage during cold sintering of ZnO with water. The displacement curve shows that cold sintering using water results in significant shrinkage with temperature increase. The maximum compaction rate can be deduced from the first derivative curve, which occurs at 170°C. Nevertheless, the maximum density achieved is 86% at 250°C as previously shown in Fig. 2. Microstructural observations of samples cold sintered at 170°C and 250°C (Fig. 3c and d) do not show morphological changes in the ZnO grains compared to the starting powder, consisting of small, rounded particles and larger prismatic ones (Fig. 3b). In addition, there is a small number of faceted grains in the cold sintered samples, and no grain growth was observed regardless of the temperature. This suggests that the observed shrinkage in the compaction curve arises due to powder compaction by particle rearrangement rather than densification during sintering. This lack of sintering could be explained by the low solubility of ZnO in water,

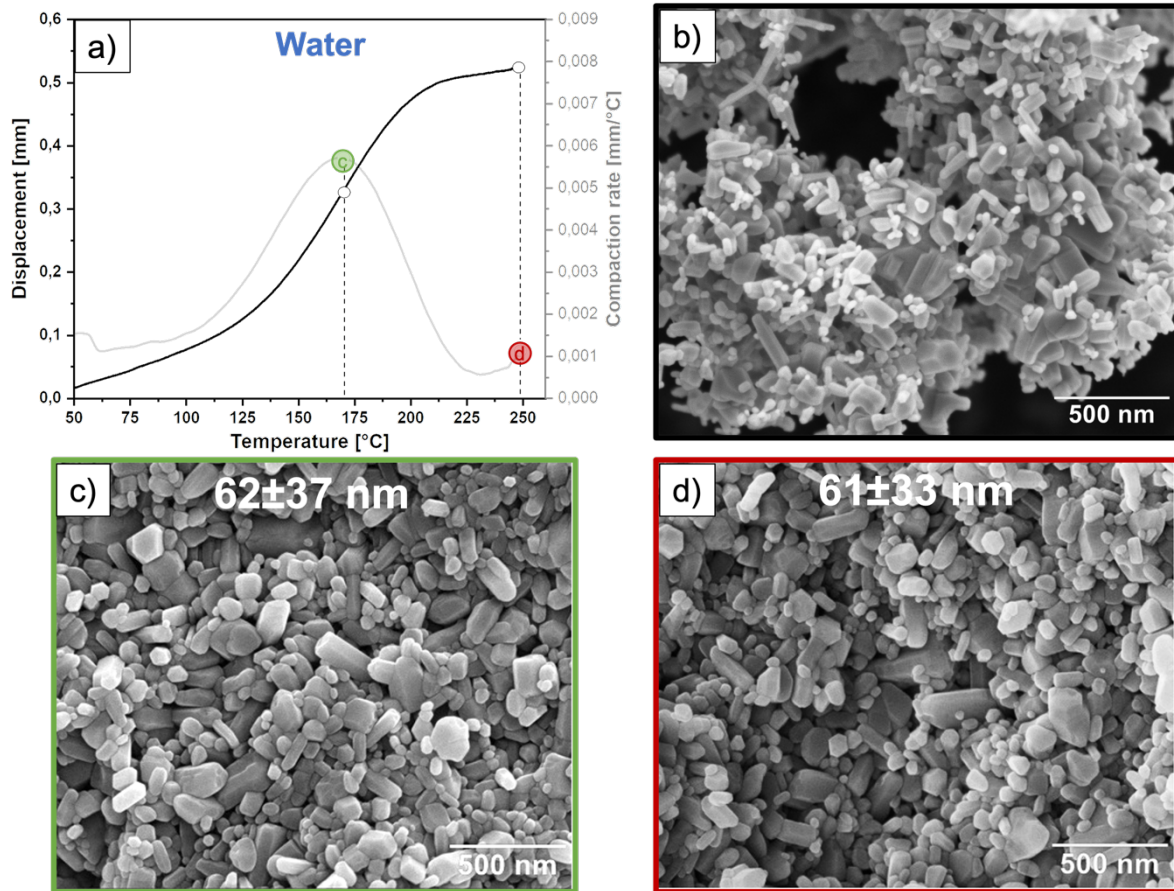and therefore, insufficient amount of mobile ionic species which are essential for the precipitation step.

Figure 3: a) Linear shrinkage during cold sintering of ZnO under a pressure of 335 MPa using pure water as a transient liquid phase, the grey curve represents the first derivative of the displacement curve; b) SEM image of the starting powder. SEM image of a fracture surface of a sample cold sintered for 1 h c) at 170°C, and d) at 250°C. The insets in c) and d) shows average grain size ± one standard deviation.

The shrinkage curve measured during CSP using acetic acid and its first derivative, which describes the rate of shrinkage, is displayed in Figure 4a. As can be seen, densification starts at a very low temperature of ~50°C and ends around 125°C. The microstructure after sintering at 70°C (Fig. 4b) consists of rounded grains connected through sintering necks. Such a pronounce morphological change from the prismatic particle shape of the starting powder indicates the activation of the dissolution step, which is absent when pure water is used as a liquid phase as shown previously. Cold sintering at 125°C (Fig 4c) results in grain growth from ~67 nm at 70°C to 133 nm with faceted grain shape. Sintering at a higher temperature of 170°C (Fig. 4d) leads to further grain growth to 155 nm. However, it is noteworthy that the

samples start to structurally deteriorate at such high temperatures. The relative density at all three temperatures (70, 125 and 170°C) is ≥ 93% after 1 h dwell time.
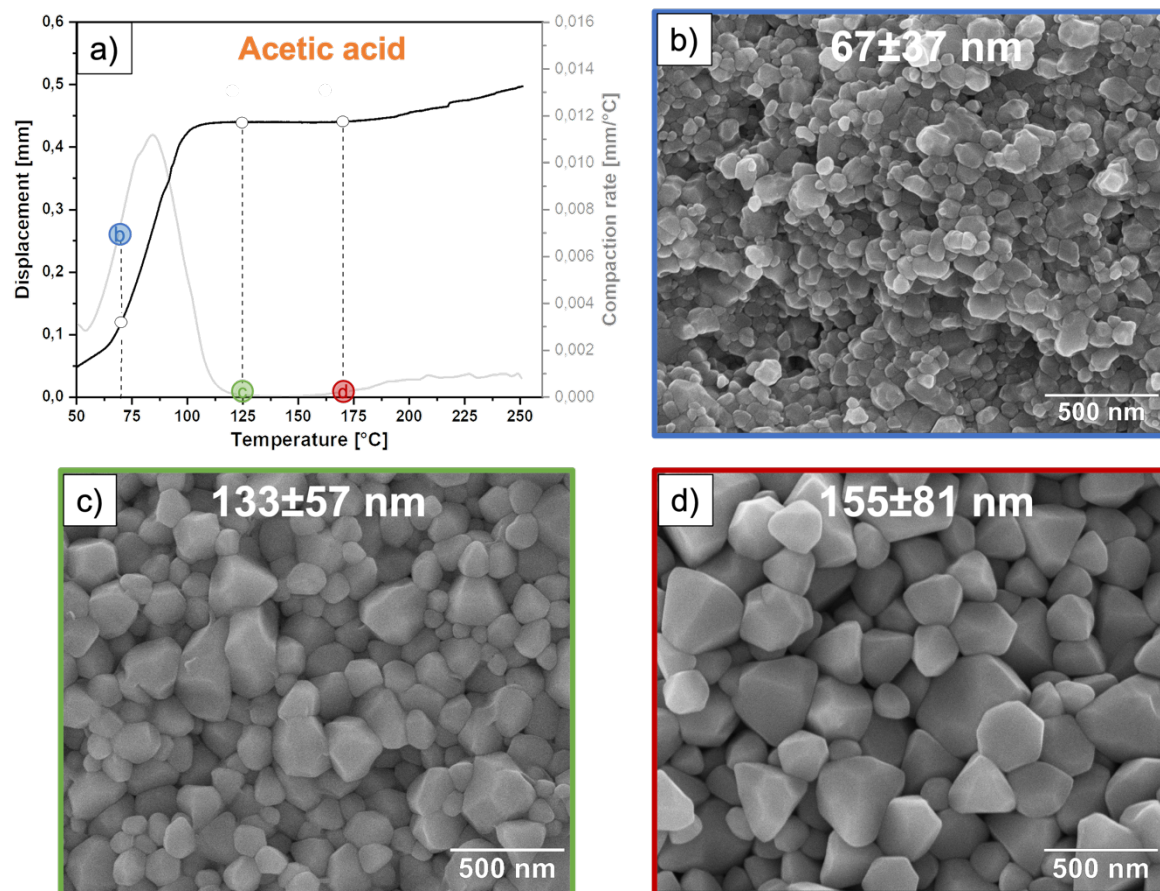

Figure 4: a) Linear shrinkage during heating to 250°C (anisothermal) in CSP of ZnO under a pressure of 335 MPa using 2M acetic acid as a transient liquid phase, the grey curve represents the first derivative of the displacement curve. Microstructure of ZnO cold sintered for 1 h at a temperature of b) 70°C, c) 125°C and d) 170°C. The inset in b, c and d) shows average grain size ± one standard deviation.

For formic acid, cold sintering kinetics start around 50°C and end at 170°C during heating as depicted by the shrinkage and compaction rate curve in Fig. 5a. The microstructure of a sample sintered at 70°C (Fig. 5b) shows compacted spherical grains in the same size range of the starting powder and with significant amount of porosity, which is in good agreement with the measured density of ≤ 83%. The shape change of the ZnO particles indicates effective dissolution activity of formic acid; however, 70°C seems to be low for driving densification mechanism and neck growth. Sintering at 125°C enhances the relative density to values above 90% and leads to the formation of well bound multifaceted grains without coarsening (Fig. 5c). At a higher temperature of 170°C, no gain in density is achieved. The microstructure is similar to the one sintered at 125°C, consisting of flat faceted grains (Fig. 5d). An important

observation is the preservation of grain size despite the temperature increase to 170°C, in contrast to the grain growth observed when cold sintering using acetic acid. This result demonstrates that grain growth observed under CSP conditions is not only controlled by temperature and time, but also by the type of the used transient liquid phase. Accordingly, cold sintering using formic acid offers an additional advantage of densifying ZnO to almost full density ~98% while maintaining the size of the initial nanometre particles.
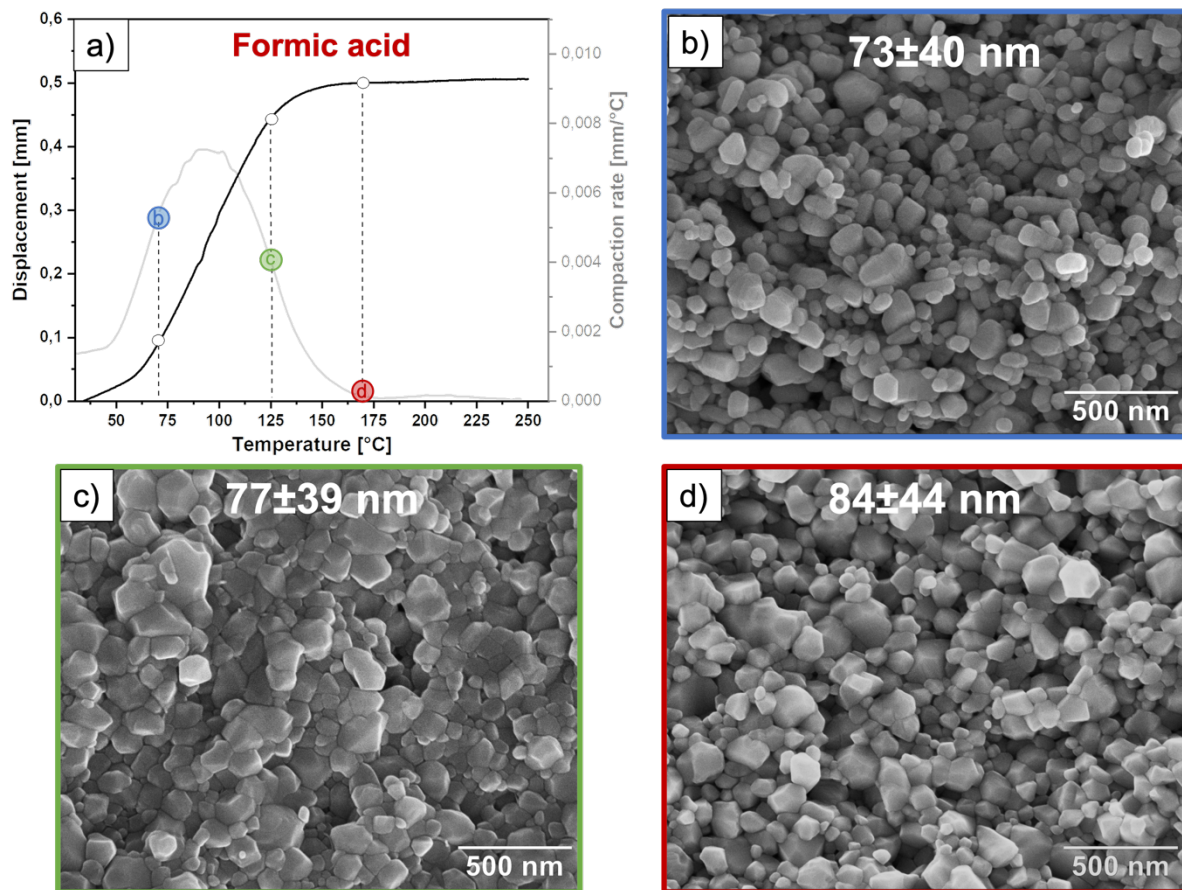

Figure 5: a) Linear shrinkage during heating to 250°C (anisothermal) in CSP of ZnO under a pressure of 335 MPa using 2M formic acid as a transient liquid phase, the grey curve represents the first derivative of the displacement curve. Microstructure of ZnO cold sintered for 1 h at a temperature of b) 70°C, c) 125°C and d) 170°C. The inset in b, c and d) shows average grain size ± one standard deviation.

Citric acid is not a compatible liquid phase for CSP of ZnO, as the relative density of samples sintered with citric acid for 1 h at 250°C is below 80%. Fig. 6a shows the compaction and its rate during heating 250°C. The compaction increases with temperature until 220°C where a reduction in the displacement and a negative compaction rate is recorded (upward movement of the pressing piston), which can be explained by pressure build-up in the sample due to decomposition of zinc citrate. Zinc citrate decomposes in the temperature range 25–

300°C by releasing water and carbon monoxide molecules [30]. Therefore, the sharp increase in the compaction rate above 225°C is likely to be related to the loss of gaseous molecules and extrusion of powder, rather than true sample shrinkage. Morphological change of the starting powder, indicative of the dissolution process, can be observed in the microstructures of samples cold sintered at 125°C and 170°C (Fig. 6b and c) At 250°C (Fig. 6d), grain faceting and coarsening occur, but no densification is observed.
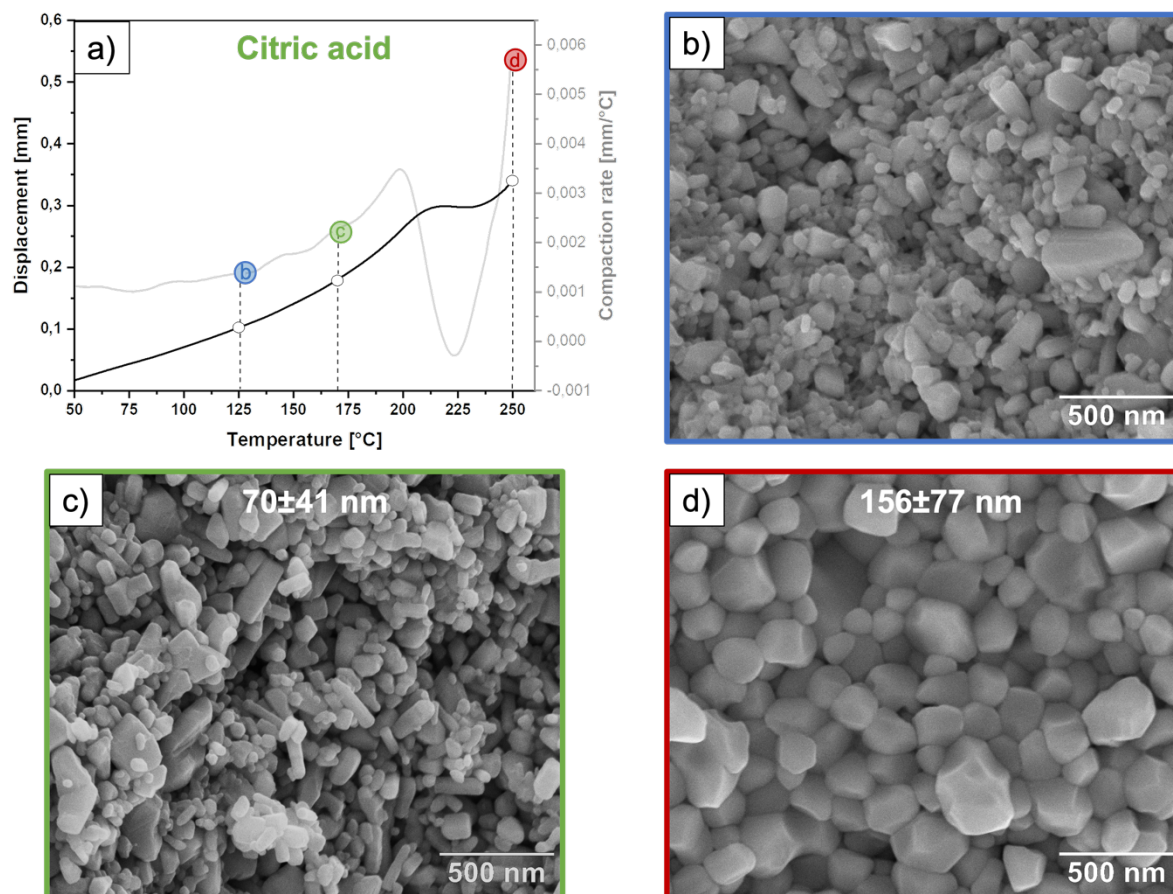

Figure 6: a) Linear shrinkage during heating to 250°C (anisothermal) in CSP of ZnO under a pressure of 335 MPa using 2M citric acid as a transient liquid phase, the grey curve represents the first derivative of the displacement curve. Microstructure of ZnO cold sintered for 1 h at a temperature of b) 125°C, c) 170°C and d) 250°C. The insets in c and d) shows the average grain size ± one standard deviation. Grain size in b) could not be measured as the microstructure was covered by the liquid phase.

3.3 Chemical interactions

Densification mechanisms acting in CSP are still under debate, but most studies on cold sintering refer to pressure solution as the main sintering mechanism [31]. It is described as a three-stage process: (1) dissolution of the solid phase into the liquid phase, which is enhanced by the external pressure; (2) diffusion of dissolved ionic species (Zn^{2+} in ZnO systems) in the
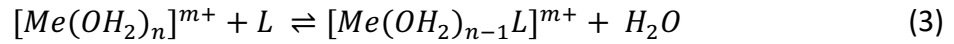
direction of low chemical potential, i.e. from highly stressed particle–particle contact areas to particles interstitials (pores), and (3) precipitation of ionic species from the supersaturated solution that evolves during liquid phase evaporation. Hence, unsuccessful densification under CSP can be attributed to the deactivation of any of these stages, and the kinetics controlled by the rate limiting mechanism of these serial processes. In our present study, the lack of densification observed with samples cold sintered using pure water can be ascribed to the low solubility of ZnO, and therefore, low concentration of Zn^{2+} that could drive the densification process below 150 C. When ZnO is dissolved in the liquid phase, Zn^{2+} rarely exist as free cations and they undergo speciation that is mainly controlled by the pH and ligands of the liquid phase [32]. In organic acids, a chelating reaction occurs between the chelating ligands in the acidic liquid phase and ZnO which results in the formation of zinc complexes. The stability of the formed complexes determines the facility for the precipitation of Zn^{2+} to ZnO.

Formic, acetic and citric acid aqueous solutions were used in this work for cold sintering ZnO. As shown in the previous section, formic and acetic acid aqueous solutions were successful in densifying ZnO to densities ≥ 95% of the theoretical, whereas citric acid showed poor densification. Regarding the solubility of ZnO in these organic acids. It is well documented that the solubility of ZnO strongly depends on the pH of the solution, such that a low or high pH value would result in an increased solubility [32]. The strength of an acid can be quantified by its pK_a value which is defined as: $pK_a = -\log(K_a)$, where K_a is the dissociation constant of the respective acid. The lower the pK_a value, the stronger the acid. The relationship between the pK_a and pH value of an acid is given by the Henderson–Haselbach equation [33]. Consequently, an acid with small pK_a would result in a low pH and therefore higher solubility. From table 1, it can be seen that citric acid has the lowest pK_a among the acids used in this work, followed by formic and acetic acid. Accordingly, the highest solubility could be expected in citric acid. In fact, citric acid has been observed to extensively enhance the dissolution of ZnO in aqueous systems, owing to the polydenticity of the citrate ligand which forms strong coordinating complexes with ZnO [34]. This complex formation between the Zn^{2+} cations and the citrate weakens the metal oxide bond, resulting in a higher degree of detachment and enhanced dissolution. Hence, the observed difference in the densification behaviour cannot be attributed to the dissolution step, as citric acid shows the highest dissolving ability.

When ZnO is dissolved in an aqueous solution, it undergoes different side reactions forming hydrocomplexes, such as $Zn(OH)_2$, $Zn(OH)^+$, Zn^{2+}, etc. But for simplification the net dissolution reaction can be given as:

$$ZnO_{(s)} \rightleftharpoons Zn^{2+}_{(aq)} + OH^-_{(aq)} \tag{2}$$

In organic acids, complex formation takes place which binds the Zn^{2+} ions to a ligand, L, in a chelating reaction. The complex formation can be generally described as follows:

$$[Me(OH_2)_n]^{m+} + L \rightleftharpoons [Me(OH_2)_{n-1}L]^{m+} + H_2O \tag{3}$$

where Me is the metal ion (here Zn) and L is the ligand. A measure of the strength of the bond between the ligand and metal ion can be described by the formation constant of this reaction, also known as stability constant. Table 1 compiles the stability constants for the formation of complexes resulting from the interaction with formic, acetic and citric acid. The higher the value of the formation constant, the more stable is the complex.

Table 1: Comparison of formation constants and pKa of different acids.

Complex	Formation constant Log k_1	pK$_a$ of the acid	Decomposition Temperature [°C]
Zinc formate	0.73	3.74	77
Zinc acetate	0.88	4.75	167
Zinc citrate	4.93	3.10	180

As can be deduced from table 1, the complex zinc citrate which could form when ZnO reacts with citric acid has a much higher formation constant than that of zinc formate and zinc acetate. This means that zinc citrate exhibits a high stability against the release of Zn^{2+} which is required in the precipitation step during CSP, which could explain the poor densification observed with citric acid, as the precipitation step could be deactivated due to the high stability of formed complexing chelate. In contrast to that, zinc formate shows the lowest stability, and hence, a higher tendency for precipitation and good densification behaviour. Considering these chemical aspects, formic acid represents the best compromise between dissolution and low complex stability.

Finally, a favourable chemical transient should exhibit a good coordinating ability, i.e. good adsorption of the complexing species on the ZnO surface. This property is well shown by

formic acid, making it a model system for adsorption studies of carboxylic acids to oxide surfaces [35]. In order to study the chelating effect of formic acid on ZnO, FTIR analysis was conducted.
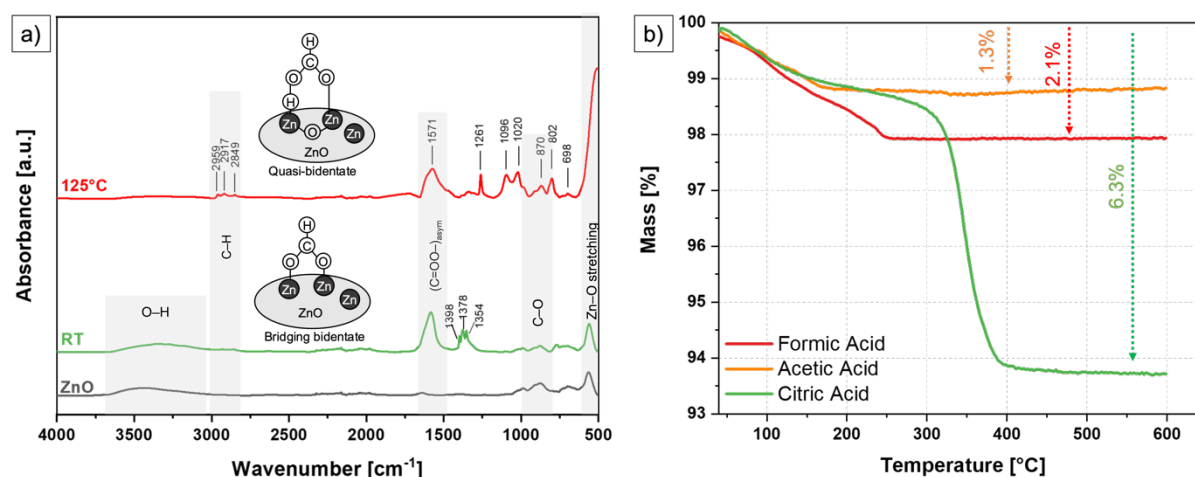

Figure 7: a) FTIR spectrum of 2M formic acid mixed with ZnO in a 13 wt% ratio at room temperature and at 125°C, the spectrum of pure ZnO is displayed as a reference. b) TGA curve showing mass loss as a function of temperature for acetic, formic and citric acid. The inset schematics in figure a) displays the coordination geometry of formic acid on ZnO.

Figure 7a shows the FTIR spectrum of formic acid mixed with ZnO at room temperature (Pre-CSP) and after cold sintering at 125°C. The broad band between 3000 and 3600 cm^{-1} is characteristic for absorption frequency of –OH [36], which indicates humidity capture and surface hydroxylation, as observed in the pure powder and the powder mixed with formic acid. This peak diminishes after cold sintering at 125°C which indicates the evaporation of the liquid phase, in accordance with intended purpose of the liquid phase to be transient in CSP. Typical FTIR spectrum of pure formic acid (not shown here) exhibits a characteristic peak at 1750 cm^{-1} which is related to the vibration frequency of the carbonyl group ($C = O$). This peak splits into two peaks that are related to the symmetric and antisymmetric stretching of the carboxyl group (COO^{-}) when it is coordinating to a metal [37]. Such splitting is observed in spectrum of the mixed powder at room temperature and in that of the cold sintered sample at 125°C. At room temperature, two peaks are observed at 1583 cm^{-1} and 1354 cm^{-1} that can be attributed to the asymmetric and symmetric COO– stretching. These frequencies are in good agreement with reported values by Lenz et al. [37], suggesting a bridging bidentate coordination geometry. After cold sintering at 125°C, the asymmetric frequency shifts to 1571 cm^{-1} which can be attributed to quasi-bidentate (unidentate) configuration [35]. This shows

the dynamic coordination character of formic acid, making it a good chelating agent– a property aspired during CSP. Another advantage of formic acid is that it is the simplest organic acid with the lowest molecular weight, resulting in low residual content of carbon after cold sintering. This is shown in the TGA curves in Fig. 7b, where formic and acetic acid have a low residual organic content, less than 2% compared to 6% in citric acid which has the highest molecular weight. Moreover, a low molecular weight is also beneficial for the adsorption of molecules on ZnO, as it minimizes steric repulsion and allows for a larger extent of adsorption.

The evolution of the chemical transients and grain boundaries after cold sintering was analysed through TEM. The microstructure after cold sintering at 70°C is shown in Fig. 8a, displaying a low-density microstructure which is in good agreement with the 82% relative density of the sample. For comparison, a low magnification TEM image of the microstructure of a sample with 95% relative density sintered at 125°C is shown in Fig. 8b, displaying a dense microstructure with a small amount of porosity. Figures 8c and d show EDS maps of samples sintered at 70°C and 125°C, respectively. The accumulation of the organic liquid phase at the surface of free grains can be observed, indicating the chelating effect. The depletion of the organic phase in the centre of the pores could be ascribed to the nucleation of new ZnO, which can be observed in Fig. 8e. A clean grain boundary between two well bounded grains is shown in Fig 8f. It is also worth noting that no amorphous phase was observed, highlighting successful densification.
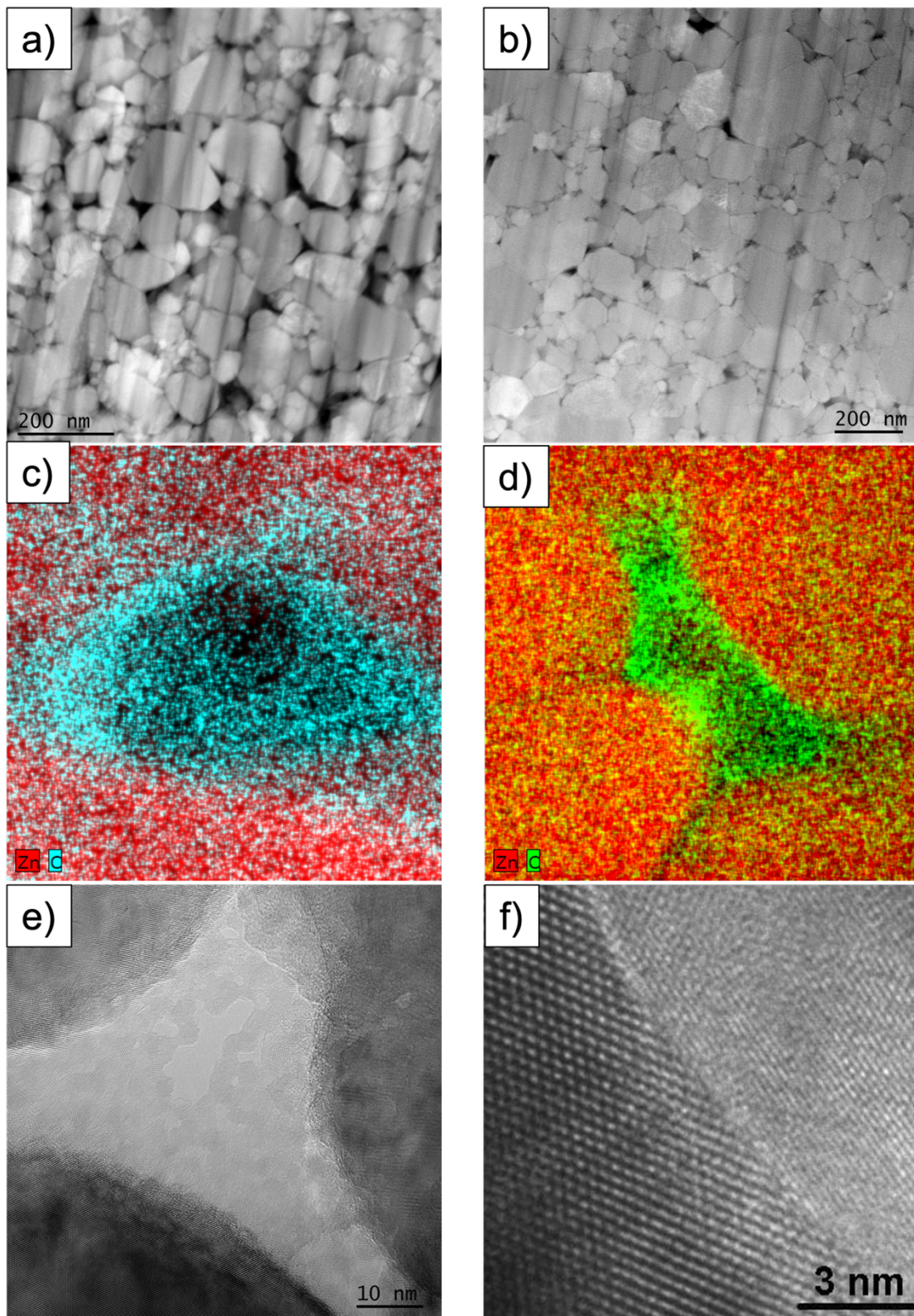
Figure 8: TEM imaging of the microstructure of cold sintered samples at (a,c,e) 70°C and (b,d,f) at 125°C. a) low magnification scanning transmission electron microscope (STEM) image of a cold sintered at 70°C with a relative density of 82%, b) STEM of a sample cold sintered at 125°C with a relative density of 95%, c) EDS mapping of a pore at 70°C, d) EDS map of pore at 125°C, e) high magnification TEM at a junction between 3 grains and f) high magnification TEM of a grain boundary after cold sintering at 125°C

3.4 Mechanical response

In this work, it has been demonstrated that high degree of densification under CSP can be achieved using aqueous solutions of formic acid and acetic acid. Acetic acid is a classical liquid phase that has been used in cold sintering studies in the literature. Other liquid phases such as aqueous solution of zinc acetate, non-aqueous dimethyl sulfoxide solutions [38] or aqueous solution of metal–organic chelates, such as zinc acetylacetonate hydrate [16], has been demonstrated. These different types of liquid phase chemistries are successful in densifying ZnO under CSP; however, the effect of the liquid phase on the mechanical strength has not been sufficiently explored yet and will be investigated in this section on the example of aqueous solutions of formic acid, acetic acid and compared to zinc acetate solution [17].

Fig. 9 shows individual failure stresses as well as the characteristic strength of each series of samples cold sintered using acetic acid, formic acid and zinc acetate. For samples cold sintered using acetic acid, a characteristic strength of σ_0= 42 [36–48] MPa and a Weibull modulus of m = 5 [3–7] were measured, where the bracketed values are the 90% confidence intervals. This strength value is relatively low compared to the results of samples cold sintered using formic acid, where a characteristic strength of σ_0= 88 [83–94] MPa and m = 8 [5–11] were measured. The strength results measured on samples sintered with formic acid are promising, as they show a ~40% higher strength than previously reported values on cold sintered ZnO using zinc acetate (σ_0= 64 [62–67] MPa and m = 8 [6–10]) [17]. It is also noteworthy that this study on cold sintering using formic acid is preliminary and does not represent an upper limit for the strength, since the processing parameters used in this work are not optimized. However, it shows the potential of enhancing the mechanical reliability of cold sintered materials by selecting an appropriate transient liquid phase.
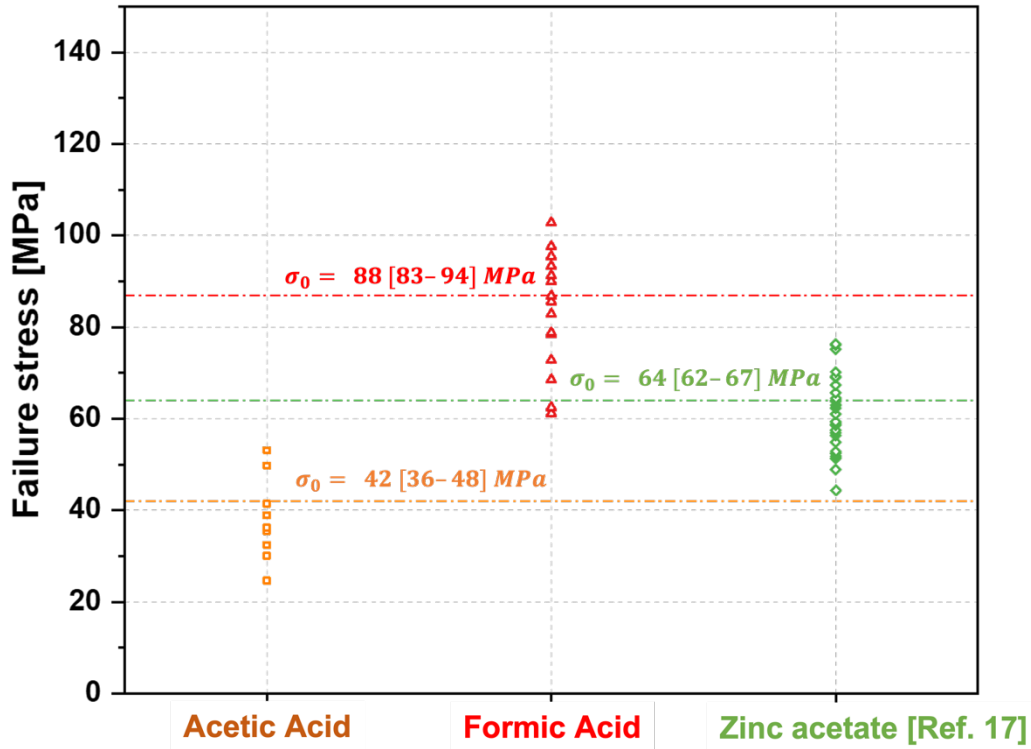
Figure 9: Biaxial fracture stress distributions for cold sintered samples using aqueous solutions of acetic acid, formic acid and zinc acetate. The characteristic strength σ_0 and the corresponding 90% confidence interval is inserted for each set. The Fracture stresses of samples cold sintered using zinc acetate were taken from the work of Lowum et al. [17].

In order to understand the reason for the remarkable difference in the strength of samples cold sintered using acetic acid and formic acid, a fractographic analysis was conducted. Fig. 10a and b shows fracture surfaces and typical defects observed in samples densified with acetic acid and formic acid solutions. In samples densified using acetic acid (Fig. 10a), fracture originates typically from delaminated regions in the microstructure. In addition, the fracture surface shows striation-like features oriented horizontally and perpendicular to the direction of pressure application, which may act as potential delamination sites and stress concentrators. This may explain the lower strength and larger scatter in the strength values (lower Weibull modulus). The occurrence of such delaminations could be attributed to anisotropic effects due to a combined action of pressure and acetic acid–ZnO interaction, for example, preferred growth of ZnO grains in the [0001]-direction in presence of zinc acetate as shown by Dargatz et al. [39]. However, no sound conclusions can be drawn, and further investigation is needed.

In the case of samples densified using formic acid, surface defects or volume defects associated with non-uniform liquid phase distribution, and hence, densification were identified as typical fracture origins. Fig. 10b shows the fracture surface after B3B testing of a sample densified using formic acid, where the failure originated from a surface defect. Compared to the samples densified with acetic acid, formic acid results in a clean microstructure with fracture surface representative of a well densified material. It may be hypothesized that the superior mechanical performance achieved with formic acid could be associated with a better grain boundary cohesion. However, fracture toughness measurements are required to verify this hypothesis and will be undertaken in a future work. Nonetheless, a rough estimation of the fracture toughness can be made from the size of the defect responsible for fracture and fracture stress. According to the Griffith criterion [40], the critical stress intensity factor acting on a flaw or fracture toughness, K_{IC}, stands in relation to the fracture stress, σ_c, according to the following equation:

$$K_{IC} = Y\sigma_c\sqrt{\pi a_c} \qquad\qquad (4)$$

where a_c is the size of the critical flaw and Y is a dimensionless geometry factors which takes into account the shape of the defect and loading configuration. The value of Y was taken as 1.12 for surface flaws and $2/\pi$ for volume defects [41]. In the case of the sample densified with acetic acid in Fig. 8a, the fracture origin is identified as a volume defect with a size of 200 µm and a failure stress of 36 MPa, resulting in an estimated fracture toughness of ~ 0.41 $MPa\sqrt{m}$. In comparison, the fracture in the sample cold sintered with formic acid (Fig. 8b) initiated from a surface defect with a size of ~18 µm at a stress of 95 MPa, resulting in an approximated fracture toughness of 0.80 $MPa\sqrt{m}$. This estimation shows that the estimated fracture toughness of formic acid sintered sample is twice as high as that of the sample cold sintered with acetic acid, which may indicate a stronger grain boundary cohesion. Notwithstanding, this estimation does not substitute accurate fracture toughness measurement that are needed for drawing conclusive results.
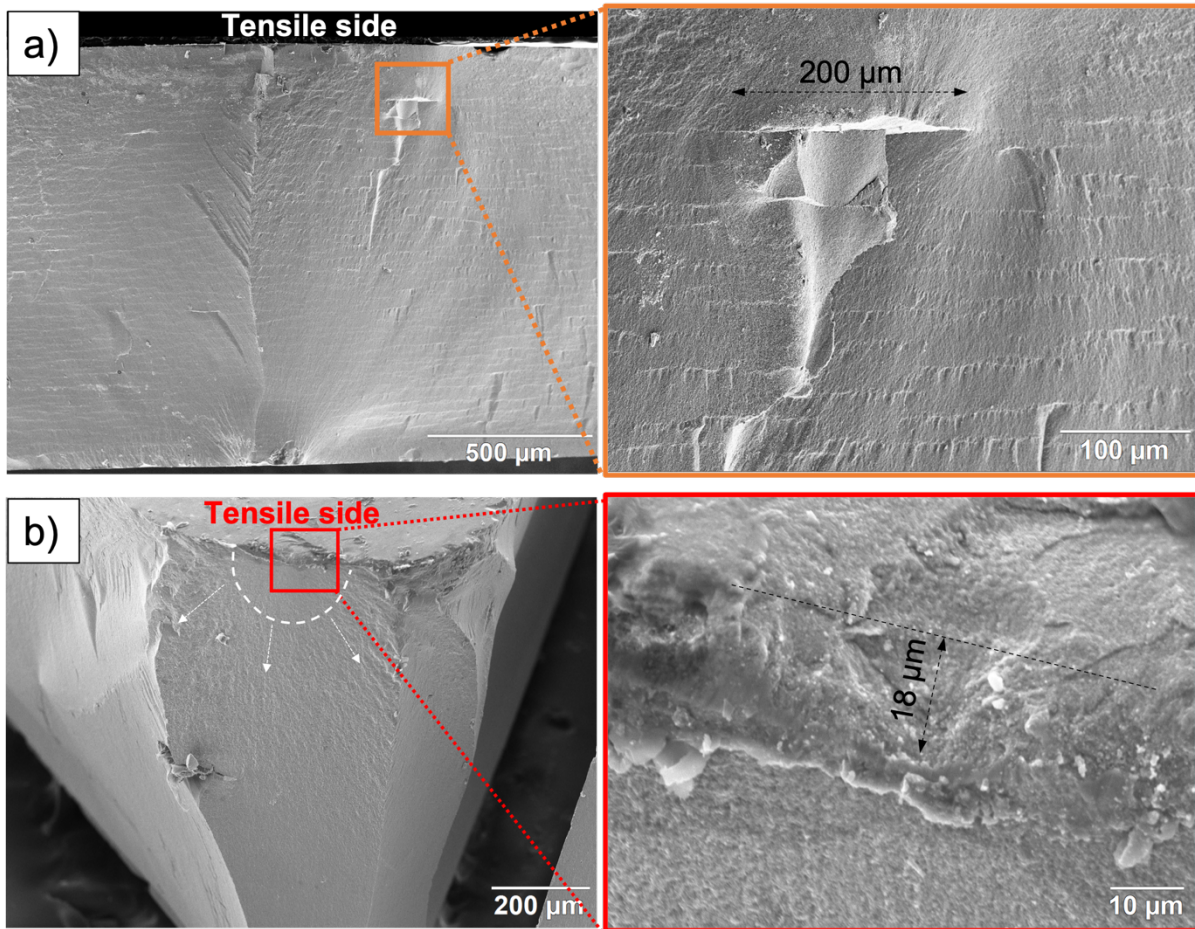
Figure 10: Fracture surfaces and enlarged view of fracture origins in: a) sample cold sintered with acetic acid solution. The sample had a failure stress of 36 MPa. The fracture origin is a delaminated area in the subsurface. b) cold sintered with formic acid solution with a failure stress of 95 MPa. The fracture origin is identified as a surface flaw.

In summary, it has been demonstrated that the type of the liquid phase used in CSP has an influence on the mechanical strength of the material. While many liquid phases may yield high densities, the mechanical strength may not be guaranteed as shown in the case of ZnO densified with acetic acid solution. The selection of formic acid as a transient liquid phase for CSP is a first step toward enhancing the reliability of cold sintered samples as shown by the promising results in this work. Optimization of the processing parameters and reduction of processing induced defects, such as delamination and non-uniform densification, by controlling thermal and pressure gradients will be investigated in future work.

4 Conclusions

Cold sintering of ZnO to relative densities above 95% at temperatures below 125°C using a 2M aqueous solutions of formic acid and acetic acid is demonstrated. Compared to densification using acetic acid, where significant grain growth was observed, samples densified using formic acid retain their grain size over temperature increase. Microstructural observation based on TEM analyses show that densification using formic acid can be driven by precipitation and nucleation of new ZnO grains in pore regions. The importance of the precipitation step for driving densification is demonstrated by a comparison study using citric acid. Even though a high dissolution rate of ZnO in citric acid is expected, no densification under CSP could be achieved, which is explained by the high stability of the zinc citrate complex, impeding the precipitation step. In contrast, zinc formate and zinc acetate complexes have much lower stability which allows the release of Zn^{2+} in the precipitation step, yielding to high densification when acetic acid and formic acid are used as transient liquid phases for CSP. Despite the similar densities, the biaxial characteristic strength of samples cold sintered using formic was twice the strength of acetic acid sintered samples and is about 40% higher than the previously reported strength in the literature using zinc acetate. This highlights the importance of the choice of transient solvent in CSP affecting the mechanical performance. This study proposes formic acid as a favourable liquid phase for CSP and represents a first step toward optimizing the mechanical reliability of cold sintered ZnO materials.

5 Significance of the results

The results presented in this work advance our understanding about the role of chemical transients in the CSP and highlight their effect on the mechanical performance of cold sintered parts. It was shown that a proper selection of the transient liquid phase can yield a remarkable improvement of strength. The fractographic analysis revealed that delaminations are prominent fracture origins in cold sintered samples, which required further investigations to explain and mitigate their occurrence. This initiated a second project in collaboration with Dr. Clive's and Dr. McKinstry's research groups in PSU on studying the occurrence of delaminations under cold sintering conditions. Using an advanced ultrasonic non-destructive testing on samples sintered with different heating rates and tool qualities, revealed that delaminations occurred due to thermal and pressure gradients during CSP.

The results achieved during my stay at PSU will be published soon in two articles under the following titles and abstracts:

Role of chemical interaction of organic acids with ZnO on the densification during the cold sintering process

Abdullah Jabr[1,*], Julian Fanghanel[2,3], Zhongming Fan[3], Raul Bermejo[1,2], Clive Randall[2,3]

[1]Department of Materials Science, Montanuniversität Leoben, Franz Josef-Strasse 18, A-8700 Leoben, Austria

[2]Materials Science and Engineering Department, The Pennsylvania State University, University Park, PA 16802, USA

[3]Materials Research Institute, Millennium Science Complex, University Park, PA 16802, USA

[*]Corresponding author's email: abdullah.jabr@unileoben.ac.at

Abstract

Cold sintering is a chemomechanical assisted densification process which allows densifying ceramics at low temperatures not exceeding 300 °C. This substantial reduction in the sintering temperature is accomplished by the aid of an externally applied pressure and a compatible transient chemical phase. In this paper, ZnO was cold sintered using various organic acids, in the following molecular complexities: formic, acetic and citric acid. The effect of these different transient phases on densification, transient chemical changes, microstructural evolution and mechanical response of the cold sintered samples was all investigated. To aid the chemical transients in the cold sintering, Fourier transform infrared spectroscopy (FTIR), thermogravimetric analyses (TGA) and transmission electron microscopy (TEM) were conducted. The results show that high relative densities (~ 96%) are achieved by formic and acetic acid, while poor densification is observed for citric acid (< 80%), despite the much higher solubility of the later. This is explained in terms of the stability of the carboxylates formed by the respective liquid phases, which highlights the importance of the precipitation step during the cold sintering process.

Effect of temperature gradients and load transfer on the densification of cold sintered parts

Abdullah Jabr[1,*], Haley N. Jones[2], Andrea P. Argüelles[3], Susan Trolier-McKinstry[2], Raul Bermejo[1,2], Clive Randall[2,4]

[1]Department of Materials Science, Montanuniversitaet Leoben, Franz Josef-Strasse 18, A-8700 Leoben, Austria
[2]Materials Science and Engineering Department, The Pennsylvania State University, University Park, PA 16802, USA
[3]Department of Engineering Science and Mechanics, Penn State University, University Park, PA 16801, USA
[4]Materials Research Institute, Millennium Science Complex, University Park, PA 16802, USA
[*]Corresponding author's email: abdullah.jabr@unileoben.ac.at

Abstract

The recently developed cold sintering process (CSP) allows densification of ceramics at remarkably low temperatures (< 300°C) in the presence of a transient liquid phase and external applied pressure. Although CSP has been successfully deployed for densifying a wide range of functional ceramics and composites, the structural integrity of cold sintered parts remains under-explored. This paper aims to highlight the effects of temperature gradients and / or improper load transfer into the sample on the densification of cold sintered parts. Ultrasonic testing is employed for non-destructive detection of flaws and discontinuities throughout the sample. A biaxial bending method is utilized to quantify the resistance to fracture of disc samples cold sintered at different temperatures, heating rates and tool qualities. Fractographic analyses revealed macroscopic flaws (delaminations) generated by stress and/or temperature gradients during CSP as strength-limiting defects, compromising the strength of the cold sintered parts. A successful prevention of such defects is demonstrated by appropriate control of the heating rate and tooling quality to guarantee homogenous load transfer.

6 References

[1] M.N. Rahaman, Sintering of Ceramics, Taylor & Francis, 2008.

[2] H.V. Atkinson, S. Davies, Fundamental aspects of hot isostatic pressing: An overview, Metall and Mat Trans A. 31 (2000) 2981–3000. https://doi.org/10.1007/s11661-000-0078-2.

[3] Z. Zhao, V. Buscaglia, P. Bowen, M. Nygren, Spark Plasma Sintering of Nano-Crystalline Ceramics, KEM. 264–268 (2004) 2297–2300. https://doi.org/10.4028/www.scientific.net/KEM.264-268.2297.

[4] R.M. German, P. Suri, S.J. Park, Review: liquid phase sintering, J Mater Sci. 44 (2009) 1–39. https://doi.org/10.1007/s10853-008-3008-0.

[5] H. Guo, J. Guo, A. Baker, C.A. Randall, Hydrothermal-Assisted Cold Sintering Process: A New Guidance for Low-Temperature Ceramic Sintering, ACS Appl. Mater. Interfaces. 8 (2016) 20909–20915. https://doi.org/10.1021/acsami.6b07481.

[6] H. Guo, A. Baker, J. Guo, C.A. Randall, Protocol for Ultralow-Temperature Ceramic Sintering: An Integration of Nanotechnology and the Cold Sintering Process, ACS Nano. 10 (2016) 10606–10614. https://doi.org/10.1021/acsnano.6b03800.

[7] J.-P. Maria, X. Kang, R.D. Floyd, E.C. Dickey, H. Guo, J. Guo, A. Baker, S. Funihashi, C.A. Randall, Cold sintering: Current status and prospects, J. Mater. Res. 32 (2017) 3205–3218. https://doi.org/10.1557/jmr.2017.262.

[8] S. Funahashi, J. Guo, H. Guo, K. Wang, A.L. Baker, K. Shiratsuyu, C.A. Randall, Demonstration of the cold sintering process study for the densification and grain growth of ZnO ceramics, J Am Ceram Soc. 100 (2017) 546–553. https://doi.org/10.1111/jace.14617.

[9] H. Guo, A. Baker, J. Guo, C.A. Randall, Cold Sintering Process: A Novel Technique for Low-Temperature Ceramic Processing of Ferroelectrics, Journal of the American Ceramic Society. 99 (2016) 3489–3507. https://doi.org/10.1111/jace.14554.

[10] X. Zhao, J. Guo, K. Wang, T. Herisson De Beauvoir, B. Li, C.A. Randall, Introducing a ZnO–PTFE (Polymer) Nanocomposite Varistor via the Cold Sintering Process, Adv. Eng. Mater. 20 (2018) 1700902. https://doi.org/10.1002/adem.201700902.

[11] J. Guo, X. Zhao, T.H.D. Beauvoir, J.-H. Seo, S.S. Berbano, A.L. Baker, C. Azina, C.A. Randall, Recent Progress in Applications of the Cold Sintering Process for Ceramic–

Polymer Composites, Advanced Functional Materials. 28 (2018) 1801724. https://doi.org/10.1002/adfm.201801724.

[12] S. Dursun, K. Tsuji, S.H. Bang, A. Ndayishimiye, C.A. Randall, A Route towards Fabrication of Functional Ceramic/Polymer Nanocomposite Devices Using the Cold Sintering Process, ACS Appl. Electron. Mater. 2 (2020) 1917–1924. https://doi.org/10.1021/acsaelm.0c00225.

[13] X. Kang, R. Floyd, S. Lowum, M. Cabral, E. Dickey, J. Maria, Mechanism studies of hydrothermal cold sintering of zinc oxide at near room temperature, J. Am. Ceram. Soc. 102 (2019) 4459–4469. https://doi.org/10.1111/jace.16340.

[14] M.Y. Sengul, J. Guo, C.A. Randall, A.C.T. van Duin, Water-Mediated Surface Diffusion Mechanism Enables the Cold Sintering Process: A Combined Computational and Experimental Study, Angew. Chem. Int. Ed. 58 (2019) 12420–12424. https://doi.org/10.1002/anie.201904738.

[15] R.D. Floyd, S. Lowum, J.-P. Maria, Cold sintering zinc oxide with a crystalline zinc acetate dihydrate mass transport phase, J Mater Sci. 55 (2020) 15117–15129. https://doi.org/10.1007/s10853-020-05100-9.

[16] A. Ndayishimiye, Z. Fan, S. Funahashi, C.A. Randall, Assessment of the Role of Speciation during Cold Sintering of ZnO Using Chelates, Inorg. Chem. 60 (2021) 13453–13460. https://doi.org/10.1021/acs.inorgchem.1c01806.

[17] S. Lowum, R. Floyd, R. Bermejo, J.-P. Maria, Mechanical strength of cold-sintered zinc oxide under biaxial bending, J Mater Sci. 54 (2019) 4518–4522. https://doi.org/10.1007/s10853-018-3173-8.

[18] K. Nur, M. Zubair, J.S.K.-L. Gibson, S. Sandlöbes-Haut, J. Mayer, M. Bram, O. Guillon, Mechanical properties of cold sintered ZnO investigated by nanoindentation and micro-pillar testing, Journal of the European Ceramic Society. (2021) S0955221921007202. https://doi.org/10.1016/j.jeurceramsoc.2021.10.011.

[19] R. Floyd, S. Lowum, J.-P. Maria, Instrumentation for automated and quantitative low temperature compaction and sintering, Review of Scientific Instruments. 90 (2019) 055104. https://doi.org/10.1063/1.5094040.

[20] S.H. Bang, A. Ndayishimiye, C.A. Randall, Anisothermal densification kinetics of the cold sintering process below 150 °C, J. Mater. Chem. C. 8 (2020) 5668–5672. https://doi.org/10.1039/D0TC00395F.

[21] E. Standards, BS EN 1389:2003 Advanced technical ceramics-Ceramic composites-Physical properties-Determination of density and apparent porosity, Https://Www.En-

Standard.Eu. (n.d.). www.en-standard.eu/bs-en-1389-2003-advanced-technical-ceramics-ceramic-composites-physical-properties-determination-of-density-and-apparent-porosity/.

[22] PubChem, ZINC oxide, (n.d.). https://pubchem.ncbi.nlm.nih.gov/compound/14806 (accessed August 18, 2022).

[23] A. Börger, P. Supancic, R. Danzer, The ball on three balls test for strength testing of brittle discs: stress distribution in the disc, Journal of the European Ceramic Society. 22 (2002) 1425–1436. https://doi.org/10.1016/S0955-2219(01)00458-7.

[24] H.N. Yoshimura, A.L. Molisani, N.E. Narita, J.L.A. Manholetti, J.M. Cavenaghi, Mechanical Properties and Microstructure of Zinc Oxide Varistor Ceramics, (n.d.) 6.

[25] W. Weibull, A Statistical Distribution Function of Wide Applicability, J. Appl. Mech. 18 (1951) 253.

[26] Advanced technical ceramics - Monolithic ceramics - Mechanical tests at room temperature - Part 5: Statistical analysis, (1997).

[27] K. Nur, T.P. Mishra, J.G.P. da Silva, J. Gonzalez-Julian, M. Bram, O. Guillon, Influence of powder characteristics on cold sintering of nano-sized ZnO with density above 99 %, Journal of the European Ceramic Society. 41 (2021) 2648–2662. https://doi.org/10.1016/j.jeurceramsoc.2020.11.007.

[28] J. Gonzalez-Julian, K. Neuhaus, M. Bernemann, J. Pereira da Silva, A. Laptev, M. Bram, O. Guillon, Unveiling the mechanisms of cold sintering of ZnO at 250 °C by varying applied stress and characterizing grain boundaries by Kelvin Probe Force Microscopy, Acta Materialia. 144 (2018) 116–128. https://doi.org/10.1016/j.actamat.2017.10.055.

[29] J. Liang, X. Zhao, S. Kang, J. Guo, Z. Chen, Y. Long, Q. Zeng, J. Sun, L. Yang, R. Liao, C.A. Randall, Microstructural evolution of ZnO via hybrid cold sintering/spark plasma sintering, Journal of the European Ceramic Society. 42 (2022) 5738–5746. https://doi.org/10.1016/j.jeurceramsoc.2022.06.069.

[30] A. Srivastava, V.G. Gunjikar, A.P.B. Sinha, Thermoanalytical studies of zinc citrate, bismuth citrate and calcium citrate, Thermochimica Acta. 117 (1987) 201–217. https://doi.org/10.1016/0040-6031(87)88115-7.

[31] A. Ndayishimiye, M.Y. Sengul, T. Sada, S. Dursun, S.H. Bang, Z.A. Grady, K. Tsuji, S. Funahashi, A.C.T. van Duin, C.A. Randall, Roadmap for densification in cold sintering: Chemical pathways, Open Ceramics. 2 (2020) 100019. https://doi.org/10.1016/j.oceram.2020.100019.

[32] P. Benezeth, D.A. Palmer, D.J. Wesolowski, C. Xiao, New Measurements of the Solubility of Zinc Oxide from 150 to 350◦C, Journal of Solution Chemistry. (2002) 27.

[33] H.N. Po, N.M. Senozan, The Henderson–Hasselbalch Equation: Its History and Limitations, (n.d.) 5.

[34] R.-A.-T.P. Rupasinghe, Dissolution and aggregation of zinc oxide nanoparticles at circumneutral pH; a study of size effects in the presence and absence of citric acid, Master of Science, University of Iowa, 2011. https://doi.org/10.17077/etd.hj0p3fhm.

[35] M. Buchholz, Q. Li, H. Noei, A. Nefedov, Y. Wang, M. Muhler, K. Fink, C. Wöll, The Interaction of Formic Acid with Zinc Oxide: A Combined Experimental and Theoretical Study on Single Crystal and Powder Samples, Top Catal. 58 (2015) 174–183. https://doi.org/10.1007/s11244-014-0356-7.

[36] Riyadh M. Alwan, ZnO nanoparticles, Sol-gel, SEM & XRD, Nanoscience and Nanotechnology. (2015) 6.

[37] A. Lenz, L. Selegård, F. Söderlind, A. Larsson, P.O. Holtz, K. Uvdal, L. Ojamäe, P.-O. Käll, ZnO Nanoparticles Functionalized with Organic Acids: An Experimental and Quantum-Chemical Study, J. Phys. Chem. C. 113 (2009) 17332–17341. https://doi.org/10.1021/jp905481v.

[38] X. Kang, R. Floyd, S. Lowum, D. Long, E. Dickey, J.-P. Maria, Cold sintering with dimethyl sulfoxide solutions for metal oxides, J Mater Sci. 54 (2019) 7438–7446. https://doi.org/10.1007/s10853-019-03410-1.

[39] B. Dargatz, J. Gonzalez-Julian, O. Guillon, Anomalous coarsening of nanocrystalline zinc oxide particles in humid air, Journal of Crystal Growth. 419 (2015) 69–78. https://doi.org/10.1016/j.jcrysgro.2015.02.101.

[40] G. A. A;, VI. The phenomena of rupture and flow in solids, Philosophical Transactions of the Royal Society of London. 221 (1921) 163–198.

[41] G.D. Quinn, NIST Recommended Practice Guide Fractography of Ceramics and Glasses, National Institute of Standards and Technology, 2016. https://doi.org/10.6028/NIST.SP.960-16e2.